

A Unique Cardiac Electrophysiological 3D Model

Cristina Rueda^{1,2,*}, Alejandro Rodríguez-Collado¹, Itziar Fernández^{1,3},
Christian Canedo¹, María Dolores Ugarte⁴, and Yolanda Larriba^{1,2}

¹Department of Statistics and Operations Research, University of
Valladolid, Spain

²Mathematics Research Institute of the University of Valladolid
(IMUVA), Spain

³Biomedical Research Networking Center in Bioengineering, Biomaterials
and Nanomedicine (CIBER-BBN), Spain

⁴Healthcare Research Institute of Navarre (IdiSNA), Spain

Abstract

Mathematical models of cardiac electrical activity are one of the most important tools for elucidating information about the heart diagnostic. Even though it is one of the major problems in biomedical research, an efficient mathematical formulation for this modelling has still not been found. In this paper, we present an outstanding mathematical model. It relies on a five dipole representation of the cardiac electric source, each one associated with the well-known waves of the electrocardiogram signal. The mathematical formulation is simple enough to be easily parametrized and rich enough to provide realistic signals. Beyond the physical basis of the model, the parameters are physiologically interpretable as they characterize the wave shape, similar to what a physician would look for in signals, thus making them very useful in diagnosis. The model accurately reproduces the electrocardiogram and vectocardiogram signals of any diseased or healthy heart, bringing together different systems in a single model. Furthermore, a novel algorithm accurately identifies the model parameters. This new discovery represents a revolution in electrocardiography research, solving one of the main problems in this field. It is especially useful for the automatic diagnosis of cardiovascular diseases, patient follow-up or decision-making on new therapies.

1 Main

The development of models and algorithms for the study of the cardiac electric system helps to better understand the physical processes governing the system and helps to guide therapeutic planning. The relevance of the topic has attracted the interest of scientists from different fields, such as mathematics, physics, bioengineering and medicine.

The heart muscle is a composite tissue with a complex structure that consists of various cell types. The electric activation of the heart begins at the sinus node, where pacemaker cells activate spontaneously. The corresponding current results in the excitation of the neighbouring cells, and it then spreads, first along the atria, and then along the ventricles^{1,2}.

Generalised assumptions on cardiac electrophysiological models that date back to the 1960s (ref.³), and remain part of the conventional approach are: the electric field is represented by a single or multiple dipoles, while the total electric activity is represented by a three-dimensional vector. This vector, denoted by $\vec{D}(t)$ at time t , is the sum of all the individual dipole vectors. As the depolarization wavefront spreads through the heart, $\vec{D}(t)$ changes in magnitude and direction as a function of time. $\vec{D}(t)$ typically describes a trajectory with three loops corresponding to consecutive time segments: the P wave (atrial depolarization), the QRS complex (ventricular depolarization) and the T wave (ventricular repolarization), respectively. The loops described by the P and T waves are elliptical, while the QRS has an irregular shape⁴. Furthermore, the voltage measurements registered by the Electrocardiogram (ECG) signal are the projections of $\vec{D}(t)$ in the directions of the axes of the recording electrodes located on the thoracic surface. In general, positive (negative) signals are produced when the depolarization front propagates towards (away from) a positive electrode. The opposite happens for the repolarization front. The standard ECG has signals from 12 projections or leads recorded using 10 electrodes².

In spite of the previous assumptions, mathematical formulations for ECG signals remain quite complex. Classical formulations include differential equation systems, representing the process with more or less biophysical detail. Aside from the mathematical complexity of the model formulation, some common criticisms of these models are that they hardly generate realistic 12-lead ECG signals, and that they depend on a large number of parameters which are hardly identifiable. In practice, a meaningful parameter identification is essential.

The literature dealing with dipole models for the electric activity of the heart is very extensive^{5,6,7,8,9,10,11,12,13,14,15}. Alternative approaches dealing with specific aspects of the heart's electric activity are also too many to be easily summarised^{16,17,18,19,20,21}. Furthermore, many papers since the early 1950s have been devoted to Vectorcardiography

(VCG) models⁴. Instead of 12-lead standard ECG models, they only consider three leads scanned in quasi-orthogonal axes. However, the VCG system is not common in clinical practice as there are fewer experts trained in these signals. ECG and VCG models have contributed to an improved understanding of the functioning of the heart, but have so far had little success in convincing clinicians. In particular, they fail in an important prerequisite for clinical applications, the ability to faithfully replicate ECG recorded from any diseased or healthy heart.

Here we present a novel model, named $3DFMM_{ecg}$ that relies on the classical physiological premise: the electric source is represented by a multiple dipole model. The novelty, however, is that it assumes that $\vec{D}(t)$ combines the electric signals from exactly five different sources, which represent differentiated myocardium segments, further associated to the five fundamental waves in ECG signals. Namely, $\vec{D}(t) = \vec{d}_P(t) + \vec{d}_Q(t) + \vec{d}_R(t) + \vec{d}_S(t) + \vec{d}_T(t)$, where t represents the real time and varies in $(0, 2\pi]$ for each heartbeat. Furthermore, the new model is also based on a key idea and original assumption: $\vec{d}_J(t)$, with $J \in \{P, Q, R, S, T\}$, moves in the same plane as time progresses, and its trajectory is described as a complex FMM signal, a parametrized mathematical equation that describes an elliptical trajectory. Accordingly, the magnitude of $\vec{d}_J(t)$ in a given direction is represented by a one-dimensional FMM wave, which reflects depolarization and repolarization voltage changes. An FMM wave, $W(t, A, \alpha, \beta, \omega)$, is an equation defined in terms of four parameters²². The parameter A , a positive real number, measures the wave amplitude; α is a location parameter with values in $(0, 2\pi]$; while β , with values in $(0, 2\pi]$, describes the asymmetry degree of the wave shape and also informs when the unimodal pattern corresponds to a crest or a trough. Finally, the parameter ω , with values in $[0, 1]$, measures the sharpness of the peak. The value $\omega = 1$ corresponds to an exact sinusoidal shape. Figure 1 illustrates each parameter in a simulated ECG signal. These four parameters are wave-specific, but, while A and β are also lead-specific, α and ω are the same across leads. The role of these common parameters is essential in the modelling process. They provide connectivity between the signals from different leads thus, simplifying the model substantially. For a given lead L and wave J , the quadruple $[A_J^L, \alpha_J, \beta_J^L, \omega_J]$ describes precisely the wave shape, in the same way a physician looks at the signal. From the model definition it also follows that projections of $\vec{D}(t)$, in directions different from those in the standard 12-lead system, are also formulated as a sum of five FMM waves where α and ω do not change. Thus, the approach unifies VCG and ECG systems within a single formulation.

The inclusion of an intercept and an error term that accounts for data noise results in a powerful statistical model. To make the model identifiable and even more biologically interpretable, we assume that $\alpha_P \leq \alpha_Q \leq \alpha_R \leq \alpha_S \leq \alpha_T$. These restrictions respond to the natural depolarization order of different myocardium segments. These restrictions and the fact that the number of parameters is small, some of them common to different

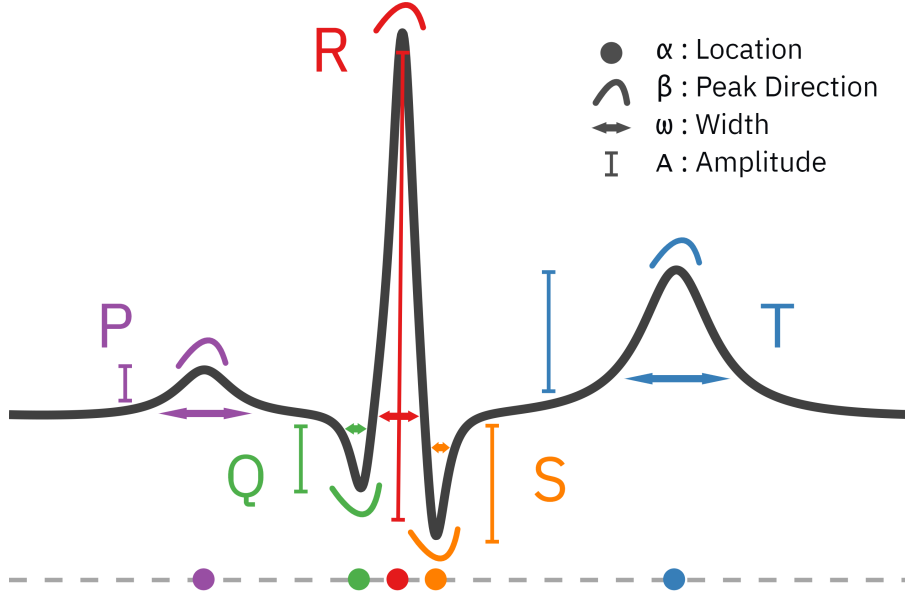


Figure 1: FMM parameter description. An ECG healthy heartbeat with waves decomposition and morphological parameter description.

leads, guarantee an accurate identification of the model parameters, even in the cases of highly anomalous patterns or noisy signals. A quadratic optimization problem must be solved to obtain the model parameters. Here, we design a backfitting iterative approach to solve the problem. Specifically, the common parameters, α and ω , are identified using a grid search. Then, the lead-specific parameter estimates A and β are easily derived using standard linear regression models. An algorithm is designed to analyse 12-lead ECG fragments of any length. In the preprocessing stage, the signal is divided beat by beat. Then, for each beat, parameter estimates are derived. The output of the algorithm provides, for each wave, the series of parameter values, corresponding to consecutive beats, which can be summarised to get average patterns as well as the changes in the patterns over time.

To evaluate the performance of the $3DFMM_{ecg}$ model, we proceed as follows. Firstly, we analysed the model's ability to reconstruct realistic ECG signals, and hence solve the forward problem, using 1D, 2D and 3D representations generated from different parameter configurations. Secondly, all the ECG fragments from patients in the PTB-XL database²³ were analysed with the new model. This database contains a great variety of anomalous, pathological and noisy cases. PTB-XL is a benchmark database, that has been used, in particular, for the challenge of Computing in Cardiology 2020 (ref.²⁴). The quality of model reconstruction is very high for the 12-lead ECG signals in most cases, something that other models are very far from reaching. Furthermore, different pathologies are associated with different parametric configurations, which indicates how the model also solves the inverse problem. Specifically, three new ECG markers are defined in terms of

the model parameters that are useful in the diagnosis. Figure 2 illustrates how the model works in a healthy heart. The choice of axes for the 2D and 3D representations is explained later on. Finally, we have designed an app (<https://fmmmodel.shinyapps.io/fmmEcg3D/>) to make it easier for researchers to check the model with their own data.

Next sections show how the $3DFMM_{ecg}$ successfully solves the main challenges of the forward and inverse problems in electrocardiography. Furthermore, a simulation study that shows how the identification algorithm provides sensible and robust parameter estimates across different configuration scenarios was conducted (see Supplementary Information). The analysis of real ECG data requires a preprocessing stage to remove baseline and other noise artifacts. Data preprocessing is detailed in the Supplementary Information.

Reconstruction of realistic ECG signals

A configuration of parameters for a healthy heart, labelled NORM, has been identified using the median values for all patients, labelled as NORM in the PTB-XL database. This configuration is used as a reference. Alternative configurations describing different pathological conditions of the heart have been generated by changing the reference values of the most relevant parameters, summarised in Table S1 of the Supplementary Information. The standard 12-lead unidimensional signals, and selected 2D and 3D representations, are provided for each configuration scenario. The axes we have selected for the 2D and 3D representations are defined as follows;

$$X = LeadII; Y = LeadII^{(i)}; Z = LeadV2 - 2 * Y$$

X is the most commonly used lead in studies, and (X, Y) is a natural bidimensional representation described by the Analytic Signal, defined in the complex plane^{25,26} (additional details are given in the Methods Section). Finally, Z has been selected after checking other alternatives, as it offers an interesting visualisation of the three loops: P , QRS and T across different patterns.

To conserve space, the figures for these configurations are shown from the Extended Data Fig. 1 to 4. In particular, the figure for the NORM configuration looks similar to Figure 2. The other configurations generate representations with characteristic and differentiated patterns.

Analysis of ECG signals from the PTB-XL database

In the preprocessing step, 210 patients (less than 1%) out of 21,837, were discarded due to very noisy patterns. Additionally, 295 patients with pacemakers were discarded due to their highly atypical but predictable ECG patterns.

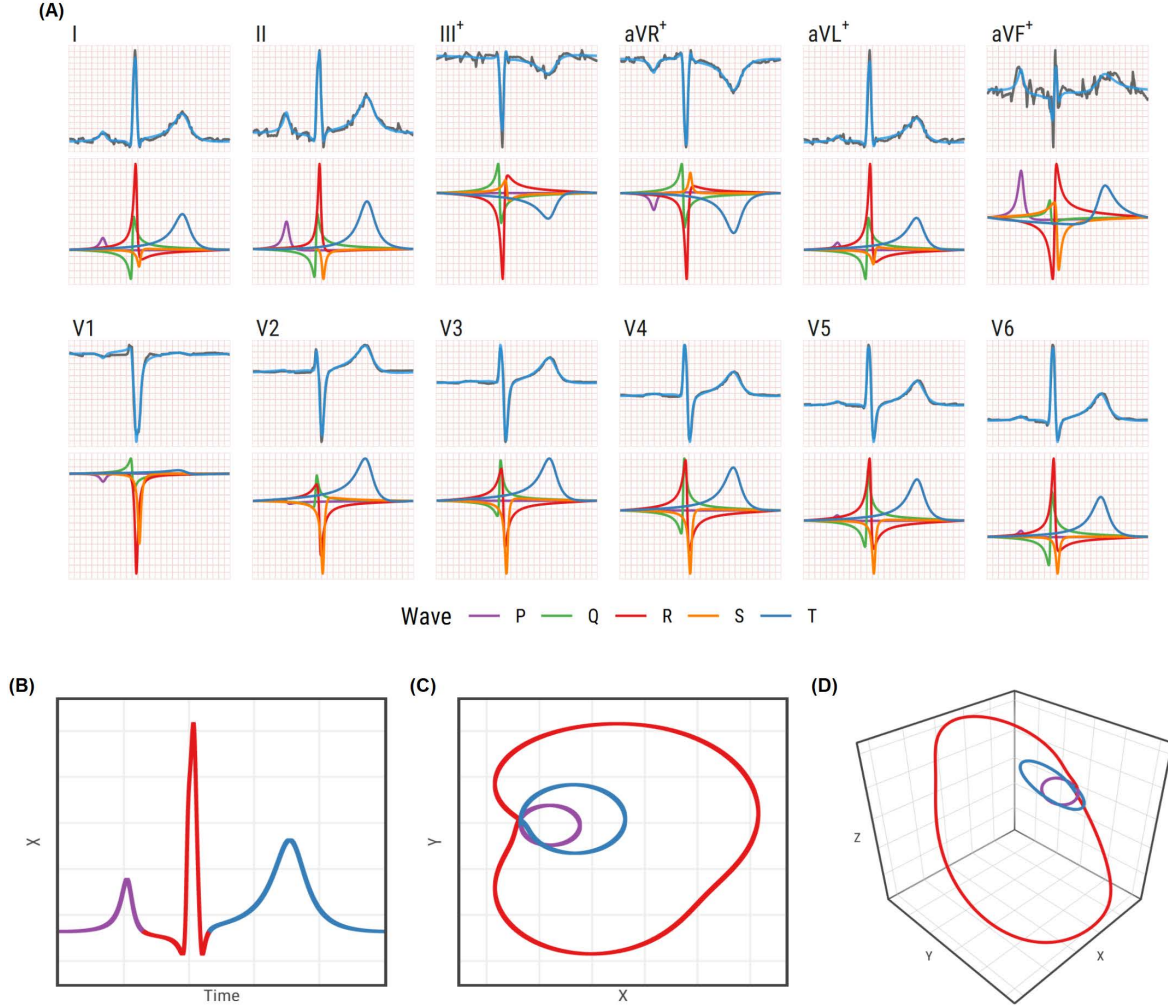


Figure 2: ECG for patient 8 in the PTB-XL database, beat n^o9. (A) 12-lead signals, using individual voltage scales (not shown). Observed (grey) and FMM predicted (blue) signals in the top panels, and wave patterns in the bottom panels. The symbol + indicates linear combinations of other signals. (B), (C) and (D): 1D, 2D and 3D representations of the predicted signals, respectively, where $X = \text{LeadII}$; $Y = \text{LeadII}^{(i)}$; $Z = \text{LeadV2} - 2 * Y$. The colours differentiate the P , QRS and T loops.

Diagnostic	N ^o	\bar{R}			$omeR$			$omeS$			$maxAR$		
		p_5	p_{50}	p_{95}	p_5	p_{50}	p_{95}	p_5	p_{50}	p_{95}	p_5	p_{50}	p_{95}
NORM	8,578	.91	.95	.97	.03	.03	.04	.02	.03	.05	525	837	1,379
CLBBB	505	.91	.96	.98	.07	.14	.21	.04	.06	.10	806	1,585	2,673
CRBBB	523	.87	.94	.97	.03	.04	.11	.04	.08	.14	396	811	1,627
HYP	599	.92	.96	.98	.03	.04	.09	.02	.03	.06	852	1,465	2,403
ALL	21,331	.92	.95	.97	.03	.04	.09	.02	.03	.07	520	888	1,677

Table 1: Statistics for selected parameters across diagnostics. Figures are a summary of the values for all patients which are, in turn, the median of the individual beat values.

A diagnostic label has been assigned to each patient in the database using SNOMED CT ontology²⁴, (bioportal.bioontology.org/ontologies/SNOMEDCT). Labels are assigned only to patients with a diagnostic likelihood of 80 or more. Some of the more recognised SNOMED labels used here are Complete Bundle Branch Blocks (CLBBB, CRBBB) left and right, respectively, and ventricular Hypertrophy (HYP).

We have calculated the model parameters for a given patient and beat. Furthermore, interesting summary measures are derived at patient level. Specifically, we define $omeR$ and $omeS$ as the median of the ω_R and ω_S individual beat values, respectively; and $maxAR$ is the maximum, across leads, of the median of the A_R individual beat values. In addition, a global model quality measure, named \bar{R} , is also obtained. It is defined as the mean, across leads, of an $R-squared$ measure, which is the proportion of variation in the signal that is explained by the model and is a common evaluation metric in regression models. Table 1 gives percentile ranges for these measures obtained across selected diagnostic classes. Specifically, normal ranges are provided. The figures in Table 1 show that the \bar{R} values are quite high across diagnostics, being higher than 90% for more than 95% of patients. On the other hand, Table 1 shows that $omeR$ and $omeS$ are good markers of CLBBB and CRBBB, respectively, while $maxAR$ is a marker for HYP, whenever $omeR$ is within the normal range. The interest of the ω FMM_{ecg} parameters in the diagnosis had already been evidenced in Rueda et al.²⁷, where simple diagnostic rules for CLBBB and CBBB (Complete Bundle Branch Block) have been defined, and can be used even when only one of the lead signals is available. Examples of observed and predicted signals from diverse heart conditions and noisy cases are given from the Extended Data Fig. 5 to 9, illustrating the ability of the model to successfully handle anomalous patterns.

Discussion

Here we present a unique cardiac electrophysiological model, the 3DFMM_{ecg}, which faithfully reconstructs the standard 12-lead ECG signal. The robustness of the method is

assessed under a variety of both pathological and noisy conditions. The model also succeeds in providing reliable quantitative results to enhance the understanding of biophysical processes, including a functional connectivity between different lead signals. A relatively small set of parameters with morphological interpretation summarises the 12-lead signals, being reliable for extrapolation and prediction, thus simplifying the diagnostic task. The model parameters are accurately estimated avoiding identifiability problems. No other model had ever come close to achieving these goals. Furthermore, the results in the paper validate the premise that the electrical source can be represented with a five two-dimensional dipole model, on which the new model is built. Interestingly, dipole models have been widely used in different forms in the literature. Another great advantage of the model is its capacity for data compression, as minimal hard disk space is needed to fully reconstruct the signal. The monitoring of patients and, in particular, telemedicine requires the storage of ECG signals and a fast on-line transmission of information^{28,29}, and therefore efficient data compression methods are in high demand.

Many challenges arise from this study. On the one hand, there is much work to do from a research perspective, such as the design of new diagnostic rules based on the FMM parameters; the identification of wave patterns specific to exceptional conditions such as atrial flutter, which do not adapt so well to the model; the integration of the new parameters in deep or machine learning procedures for classification tasks^{19,20,30,21}; or the inclusion of new terms accounting for different sources of variability. Specifically, we will start by studying a rule for HYP, using a combination of markers including the *maxAR* defined in this paper. On the other hand, there is the committed objective of getting the new markers to be used in clinical practice. To that end, devices that record the signals should provide the new markers, and more importantly, physicians need to be trained. Moreover, the current paper opens up great research opportunities for studying biological electric systems beyond the cardiac one, which have an impact on the knowledge of the effect and causes of multiple diseases, as well as the development of drugs and therapies. In particular, electric signals from other organs, such as the brain or the eyes, can be modelled using adapted 3DFMM models. Thus, the important question of analysing the relationship between signals recorded in different regions, could also be addressed with these models. Some work in this line is in progress.

Regarding the limitations, the computational time is still too high to give interactive outputs. This is due to the exhaustive search and the backfitting loop, which are time-consuming processes. However, by implementing the current method in C and using general-purpose computing on graphics processing units, the computational cost could be greatly reduced. Furthermore, the algorithm, as described here, does not identify the *P* wave when it is not located before the *QRS* complex. New research into detecting and adapting the algorithm in these cases could bring about the correct identification of the

P wave.

Methods

3DFMM_{ecg} Model

Without loss of generality, it is assumed that the time points are in $(0, 2\pi]$. In any other case, transform the time points $t' \in [t_0, T + t_0]$ to $t = \frac{(t' - t_0)2\pi}{T}$.

Let us define an FMM wave as follows: $W(t, A, \alpha, \beta, \omega) = A \cos(\phi(t, \alpha, \beta, \omega))$, where A is the wave amplitude and,

$$\phi(t, \alpha, \beta, \omega) = \beta + 2 \arctan(\omega \tan(\frac{t - \alpha}{2})), t \in (0, 2\pi] \quad (1)$$

is the wave phase.

$W(t, A, \alpha, \beta, \omega)$ is suitable for describing rhythmic up-down-up (or down-up-down) patterns, as is well justified in Rueda et al.²². The parameters characterise various morphological aspects of the wave, as detailed in the introduction.

An FMM complex signal, called Analytic Signal (AS), is defined using the Hilbert Transform (HT) as follows: $S(t) = \mu(t) + i\nu(t)$; where, $\mu(t) = W(t, A, \alpha, \beta, \omega)$, and $\nu(t) = HT(\mu(t))$. This signal has interesting properties and researchers often assume that the underlying complex signal associated to an oscillatory process is an AS (ref.²⁵). In particular, in Rueda et al.²⁶ the parametric expression for the AS is given as: $\nu(t) = \sum_{J=1}^m A_J \sin(\phi_J(t))$. Furthermore, in this paper, the AS is used to define the Y axis in 2D and 3D representations of ECG signals by considering that when $\mu^{II}(t) = P(\vec{D}(t)|LeadII)$, then $\nu^{II}(t) = P(\vec{D}(t)|LeadII^{(i)})$.

The 3DFMM_{ecg} model relies on two premises. Namely; 1.- the heart electric field originates from a multi dipole; and 2.- each dipole is represented by a vector, which moves in a plane as time progresses and is mathematically described as a complex FMM signal.

Below, we prove that the projection of such a vector is an FMM wave with the property that the values of α and ω do not depend on the direction of the projection.

Theorem

Let $\{\vec{d}(t), t \in (0, 2\pi]\}$ be a set of vectors in the same plane, \wp , and assume that the projection of $\vec{d}(t)$ in a given direction L , such as $L \in \wp$, is an FMM wave, as follows;

$$P(\vec{d}(t)|L) = M^L + W(t, A^L, \alpha^L, \beta^L, \omega^L), t \in (0, 2\pi]$$

Then, the projection of $\vec{d}(t)$ in any other direction, L' , is also an FMM wave, verifying that $\alpha^{L'} = \alpha^L$ and $\omega^{L'} = \omega^L$.

The proof of this theorem is given in the Supplementary Information.

Now, consider the tridimensional space with its origin of the central point in the chest and the voltage recorder with the ten electrodes generating the 12-lead ECG signals: $Lset = \{I, II, III, aVR, aVL, aVF, V1, V2, V3, V4, V5, V6\}$. Each of these signals is the projection of $\vec{D}(t)$ in a given direction and, in turn, the projection of $\vec{D}(t)$ is the sum of the projections of the five dipole vectors, for each of which the result of the theorem can be applied individually.

Finally, the $3DFMM_{ecg}$ model is derived, taking into account all the above considerations. Specifically, the ECG unidimensional signals are formulated as a signal plus error model in Definition 1, where the error term accounts for artefacts in the data and the intercept accounts for location changes as follows.

Definition 1. *3DFMM_{ecg} model*

$X^L(t_i)$, $t_1 < \dots < t_n$, be an observation from lead L , $L \in Lset$. Then,

$$X^L(t_i) = M^L + \sum_{J \in \{P, Q, R, S, T\}} W(t_i, A_J^L, \alpha_J, \beta_J^L, \omega_J) + e^L(t_i); \quad (2)$$

where, for $L \in Lset$, and, $J \in \{P, Q, R, S, T\}$:

- $M^L \in \mathfrak{R}$,
- $\beta_J^L \in (0, 2\pi]$,
- $\alpha_P \leq \alpha_Q \leq \alpha_R \leq \alpha_S \leq \alpha_T \leq \alpha_P$,
- $\omega_J \in [0, 1]$,
- $A_J^L \in \mathfrak{R}^+$,
- $(e^L(t_1), \dots, e^L(t_n))' \sim N_n(\mathbf{0}, \sigma^L \mathbf{I})$.

It is relevant to note that restrictions imposed on the α parameters, response to the assumption that the atrial depolarization is previous to the ventricles depolarization. Occasionally, the atria may repolarize later. In such a case, the P wave would not go before the QRS . To prevent these cases, the model can also be defined by numbering the waves and making a subsequent identification of the numbers with the letters, maintaining the relationship between the QRS and the T .

Other important parameters of practical use are the peak and trough times. They are defined as functions of the basic parameters³¹. In addition, other indices, such as the distances between waves, are easily derived from the set of basic $3DFMM_{ecg}$ model

parameters. Obtaining good estimators of these indices is crucial for clinicians because they are useful tools in the diagnosis.

Evaluation metrics

In this study, a global model quality measure, named \bar{R} , is defined for a given patient. Namely,

$$\bar{R} = \frac{1}{12} \sum_{L \in Lset} \text{median}(R_{L_b}^2),$$

where, for a fixed beat b and lead L ,

$$R_{L_b}^2 = 1 - \frac{\sum_{i=1}^n (X_b^L(t_i) - \hat{X}_b^L(t_i))^2}{\sum_{i=1}^n (X_b^L(t_i) - \bar{X}_b^L(t_i))^2}$$

is the proportion of variation in the signal that is explained by the predicted values. The higher the \bar{R} , the better the model.

Identification algorithm

The identification problem reduces to solving the following optimization problem:

$$\text{Min}_{\theta \in \Theta} \sum_{L \in Lset} \frac{1}{\sigma^L} \sum_{i=1}^n [X^L(t_i) - \mu^L(t_i, \theta)]^2,$$

where θ is the vector of the model parameters, Θ is the parametric space, and $\mu^L(t_i, \theta) = M^L + \sum_{J \in \{P, Q, R, S, T\}} W(t_i, A_J^L, \alpha_J, \beta_J^L, \omega_J)$. For a typical ECG pattern, Θ is initially defined as in Definition 1. However, Θ is reduced when atypical or very noisy patterns are analysed to achieve a correct physiological identification of waves. The values σ^L , $L \in Lset$ are identified as part of the optimization process.

For computational efficiency, the $Lset$ is reduced to $Lred = \{I, II, V1, V2, V3, V4, V5, V6\}$, as the rest of the lead signals are linear combinations of I and II . However, the weight of I and II increase by a factor of 3 in order to maintain the global weight of the derivations from the frontal plane².

From a statistical point of view, the optimization problem defined above is that of finding the Maximum Likelihood Estimates of the parameters. We adapt an iterative algorithm²⁶ to the multivariate setting. The algorithm alternates M and I steps. It is assumed that the preprocessing stage provides a QRS annotation point, denoted as t^{QRS} , for each beat. Moreover, exceptionally, one or more than one, of the eight leads are discarded in the preprocessing stage due to noise artefacts; only information on at least one of I , II , $V2$, or $V5$ lead is required. In those cases, the identification stage is conducted with the selected leads, providing estimates for the common parameters; while the estimates for the lead-specific parameters of missing leads are derived by solving a standard multiple linear regression problem at the end of each M step.

The M step obtains $K \geq 5$ FMM waves using a backfitting algorithm and the I step assigns $K \leq 5$ letters to, at most, five of these waves. Typically, $K = 5$; however, in the presence of significant noise or when the morphology is pathological, it is possible that the interesting waves may be hidden between the sixth and seventh waves (exceptionally up to the tenth). The values σ^L are updated in each iteration of the algorithm, averaging the squared difference between the expected values and the predicted values by the model. They are initially set to 1.

M step: A standard backfitting algorithm is designed by fitting a single FMM wave simultaneously to the leads in $Lred$. The fitting of a single FMM is repeated successively to the residuals. The numbers of backfitting passes programmed in each step M is five. The final estimates of M^L , A_J^L and β_J^L ; $L \in Lred$; $J \in \{P, Q, R, S, T\}$, are derived by solving a standard multiple linear regression problem.

I step: The R wave is assigned in the first I step. It corresponds to the one with the highest explained variability among those closest to t^{QRS} , which also has a positive peak on leads I or II and a negative peak in lead $V2$. In the few cases where these assumptions do not hold, additional conditions are used. Next, the preassignment of P, Q, S and T to the free components among the first five is done using $\alpha_P \leq \alpha_Q \leq \alpha_R \leq \alpha_S \leq \alpha_T$. This preassignment corresponds, in most cases, to the final assignment. However, in the presence of significant noise, or when the morphology is pathological, the interesting waves may sometimes be hidden between the sixth and seventh waves, which are checked for reassignments using thresholds on the main model parameters. In particular, noisy components are detected with too small or too high ω values.

The algorithm finishes when there is no significant increase in the objective function of the optimization problem.

In addition, the predictions from other leads in the frontal plane, III , aVL , aVR and aVF are derived using the predictions of the I and II leads, using the known linear relations between them². In the case that any of the I and II leads is tentatively eliminated in the preprocessing step, the estimates for leads in the frontal plane can be derived by solving a standard multiple linear regression problem, as is done with the missing leads in step M. A flow chart of the algorithm is given in the Extended Data Fig. 10.

Data and Code availability

This work makes use of the PTB-XL database³² that is publicly available at Physionet³³.

All the presented results are reproducible through the 3DFMM_{ecg} app, publicly available at <https://fmmmodel.shinyapps.io/fmmEc3D/>, as it implements the API used for the analyses. A detailed description of the 3DFMM_{ecg} app, including implementation

and usage examples, is provided in the Supplementary Information. The corresponding author will provide the source code upon reasonable request.

References

- [1] Malmivuo, J. & Plonsey, R. *Bioelectromagnetism - Principles and Applications of Bioelectric and Biomagnetic Fields* (Oxford University Press, USA, 1995).
- [2] Bayes de Luna, A. *Basic Electrocardiography* (John Wiley & Sons, 2007).
- [3] Holt JR, J., Barnard, A. C., Lynn, M. S. & Svendsen, P. A study of the human heart as a multiple dipole electrical source: I. normal adult male subjects. *Circulation* **40**, 687–696 (1969).
- [4] Jaros, R., Martinek, R. & Danys, L. Comparison of different electrocardiography with vectorcardiography transformations. *Sensors* **19**, 3072 (2019).
- [5] Clayton, R. *et al.* Models of cardiac tissue electrophysiology: progress, challenges and open questions. *Progress in biophysics and molecular biology* **104**, 22–48 (2011).
- [6] Balakrishnan, M., Chakravarthy, V. S. & Guhathakurta, S. Simulation of cardiac arrhythmias using a 2d heterogeneous whole heart model. *Frontiers in physiology* **6**, 374 (2015).
- [7] El Houari, K. *et al.* A fast model for solving the ecg forward problem based on an evolutionary algorithm. In *2017 IEEE 7th International Workshop on Computational Advances in Multi-Sensor Adaptive Processing (CAMSAP)*, 1–5 (IEEE, 2017).
- [8] Quarteroni, A. L. F., Manzoni, A. & Vergara, C. The cardiovascular system: mathematical modelling, numerical algorithms and clinical applications. *Acta Numerica* **26**, 365–590 (2017).
- [9] Niederer, S. A., Lumens, J. & Trayanova, N. A. Computational models in cardiology. *Nature Reviews Cardiology* **16**, 100–111 (2019).
- [10] Quiroz-Juárez, M. A., Jiménez-Ramírez, O., Aragón, J. L., Del Río-Correa, J. L. & Vázquez-Medina, R. Periodically kicked network of rlc oscillators to produce ecg signals. *Computers in biology and medicine* **104**, 87–96 (2019).
- [11] Whittaker, D. G., Clerx, M., Lei, C. L., Christini, D. J. & Mirams, G. R. Calibration of ionic and cellular cardiac electrophysiology models. *Wiley Interdisciplinary Reviews: Systems Biology and Medicine* **12**, e1482 (2020).
- [12] Versaci, M., Angiulli, G. & La Foresta, F. A modified heart dipole model for the generation of pathological ecg signals. *Computation* **8**, 92 (2020).

- [13] Corrado, C. *et al.* Using cardiac ionic cell models to interpret clinical data. *WIREs Mechanisms of Disease* **13**, e1508 (2021).
- [14] Dasgupta, S., Das, S. & Bhattacharya, U. Cardiogan: An attention-based generative adversarial network for generation of electrocardiograms. In *2020 25th International Conference on Pattern Recognition (ICPR)*, 3193–3200 (IEEE, 2021).
- [15] Cheffer, A., Savi, M. A., Pereira, T. L. & de Paula, A. S. Heart rhythm analysis using a nonlinear dynamics perspective. *Applied Mathematical Modelling* **96**, 152–176 (2021).
- [16] Schläpfer, J. & Wellens, H. J. Computer-interpreted electrocardiograms: benefits and limitations. *Journal of the American College of Cardiology* **70**, 1183–1192 (2017).
- [17] Nayak, S. K., Bit, A., Dey, A., Mohapatra, B. & Pal, K. A review on the non-linear dynamical system analysis of electrocardiogram signal. *Journal of healthcare engineering* **2018** (2018).
- [18] Satija, U., Ramkumar, B. & Manikandan, M. S. A review of signal processing techniques for electrocardiogram signal quality assessment. *IEEE reviews in biomedical engineering* **11**, 36–52 (2018).
- [19] Hannun, A. Y. *et al.* Computer-interpreted electrocardiograms: benefits and limitations. *Nature Medicine* **25**, 65–69 (2019).
- [20] Han, X. *et al.* Deep learning models for electrocardiograms are susceptible to adversarial attack. *Nature Medicine* **26**, 360–363 (2020).
- [21] Siontis, K., Noseworthy, P., Attia, Z. & Friedman, P. Artificial intelligence-enhanced electrocardiography in cardiovascular disease management. *Nature Reviews Cardiology* **18**, 465–478 (2021).
- [22] Rueda, C., Larriba, Y. & Peddada, S. Frequency modulated möbius model accurately predicts rhythmic signals in biological and physical sciences. *Scientific Reports* **9**, 1–10 (2019).
- [23] Wagner, P. *et al.* Ptb-xl, a large publicly available electrocardiography dataset. *Scientific Data* **7**, 1–15 (2020).
- [24] Perez Alday, E. A. *et al.* Classification of 12-lead ecgs: the physionet/computing in cardiology challenge 2020. *Physiological Measurement* **41**, 124003 (2021).
- [25] Sandoval, S. & De Leon, P. L. The instantaneous spectrum: A general framework for time-frequency analysis. *IEEE Transactions on Signal Processing* **66**, 5679–5693 (2018).

- [26] Rueda, C., Rodríguez-Collado, A. & Larriba, Y. A novel wave decomposition for oscillatory signals. *IEEE Transactions on Signal Processing* **69**, 960–972 (2021).
- [27] Rueda, C., Fernández, I., Larriba, Y., Rodríguez-Collado, A. & Canedo, C. Compeling new markers for automatic diagnosis. *Preprint at <https://arxiv.org/abs/2112.12196>* (2021).
- [28] Bhalerao, S., Ansari, I. A., Kumar, A. & Jain, D. K. A reversible and multipurpose ecg data hiding technique for telemedicine applications. *Pattern Recognition Letters* **125**, 463–473 (2019).
- [29] Bhaskar, S. *et al.* Designing futuristic telemedicine using artificial intelligence and robotics in the covid-19 era. *Frontiers in Public Health* **8**, 708 (2020).
- [30] Xue, J. & Yu, L. Applications of machine learning in ambulatory ecg. *Hearts* **2**, 472–494 (2021).
- [31] Rueda, C., Larriba, Y. & Lamela, A. The hidden waves in the ecg uncovered revealing a sound automated interpretation method. *Scientific reports* **11**, 1–11 (2021).
- [32] Wagner, P., Strodthoff, N., Bousseljot, R.-D., Samek, W. & Schaeffter, T. Ptb-xl, a large publicly available electrocardiography dataset (version 1.0.1). *PhysioNet* (2020). URL <https://doi.org/10.13026/x4td-x982>.
- [33] Goldberger, A. L. *et al.* Physiobank, physiotoolkit, and physionet. *Circulation* **101**, e215–e220 (2000).

Acknowledgements

The authors gratefully acknowledge the financial support received by the Spanish Ministry of Science, Innovation and Universities [PID2019-106363RB-I00 to C.R., I.F. and Y.L.].

Author contributions

C.R. conceived the aims, theoretical proposal, mathematical model developments and wrote the manuscript. C.R. and A.R.-C. developed the design and implementation of the identification algorithm. C.R., Y.L. and I.F. designed the preprocessing stage and the simulations. A.R.-C. and C.C. developed the computational code and the app. M.D.U provided critical feedback on the manuscript. All the authors revised and approved the manuscript.

Competing Interests

The authors declare no competing interests.

Additional information

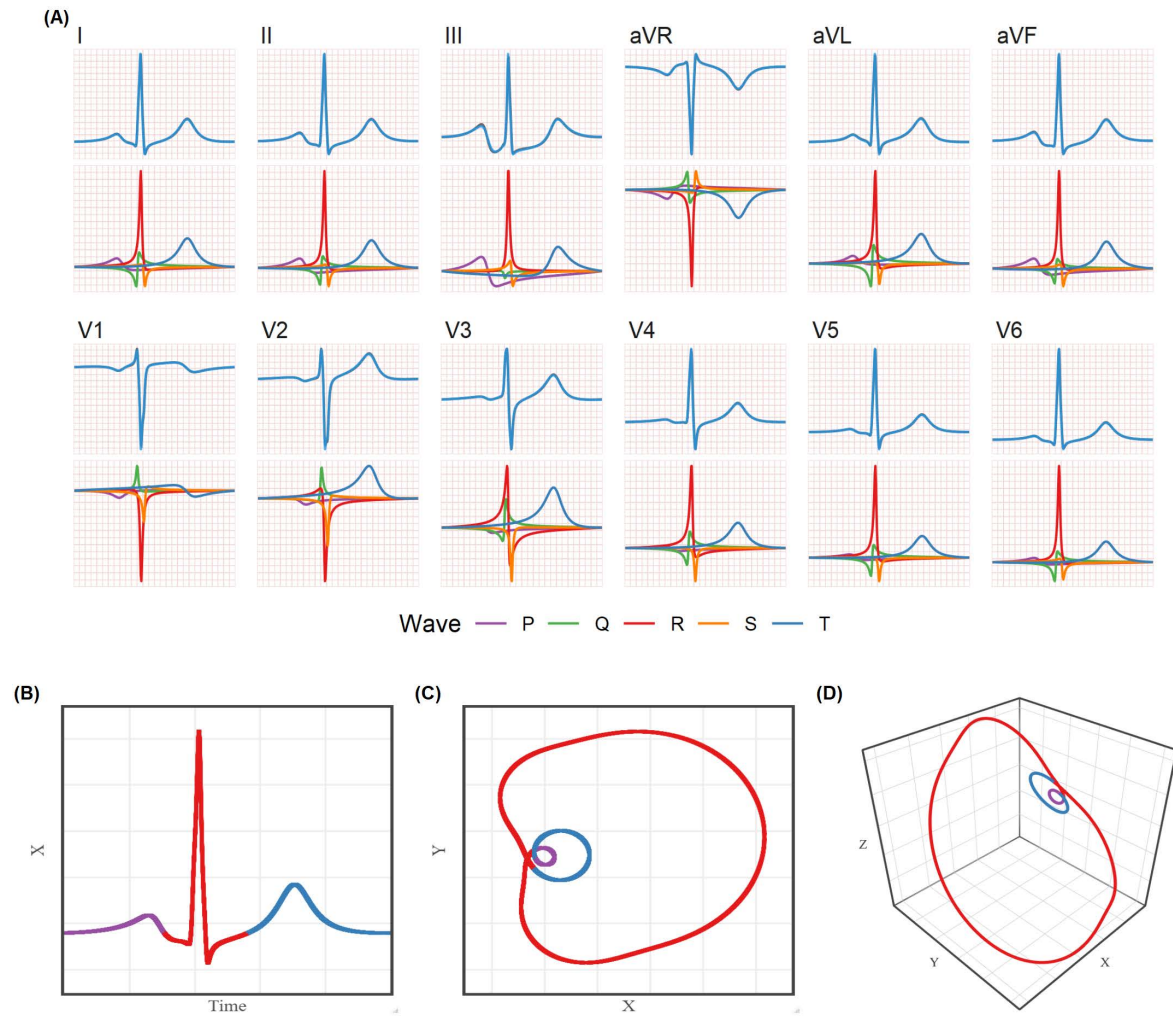
Supplementary Information

This file contains a data preprocessing overview, the Theorem's proof, a simulation study and a description of the 3DFMM_{ecg} app.

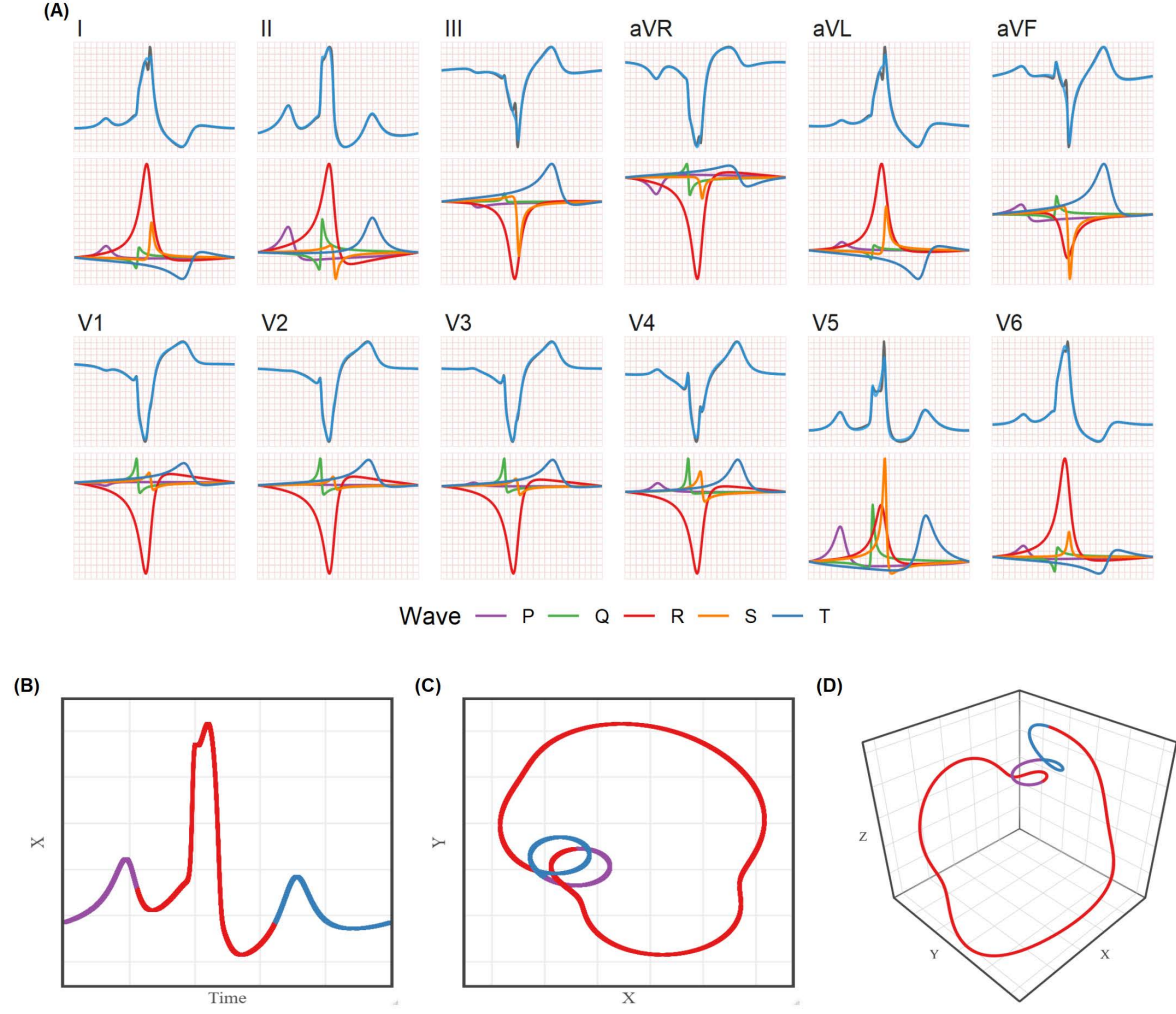
Materials & Correspondence

Correspondence and requests for materials should be addressed to Dr. Rueda. email: `cristina.rueda@uva.es`

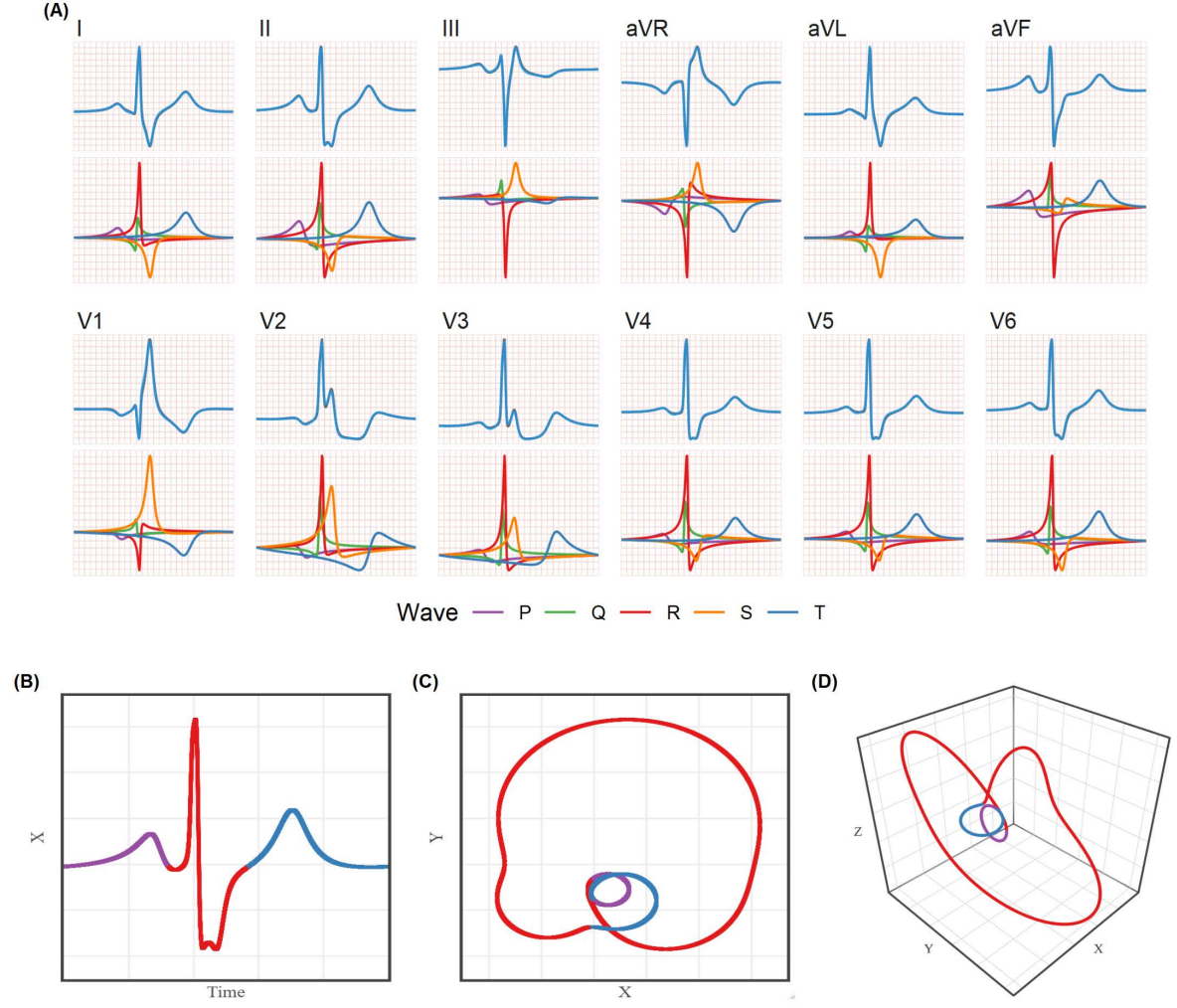
Extended Data Figures and Tables



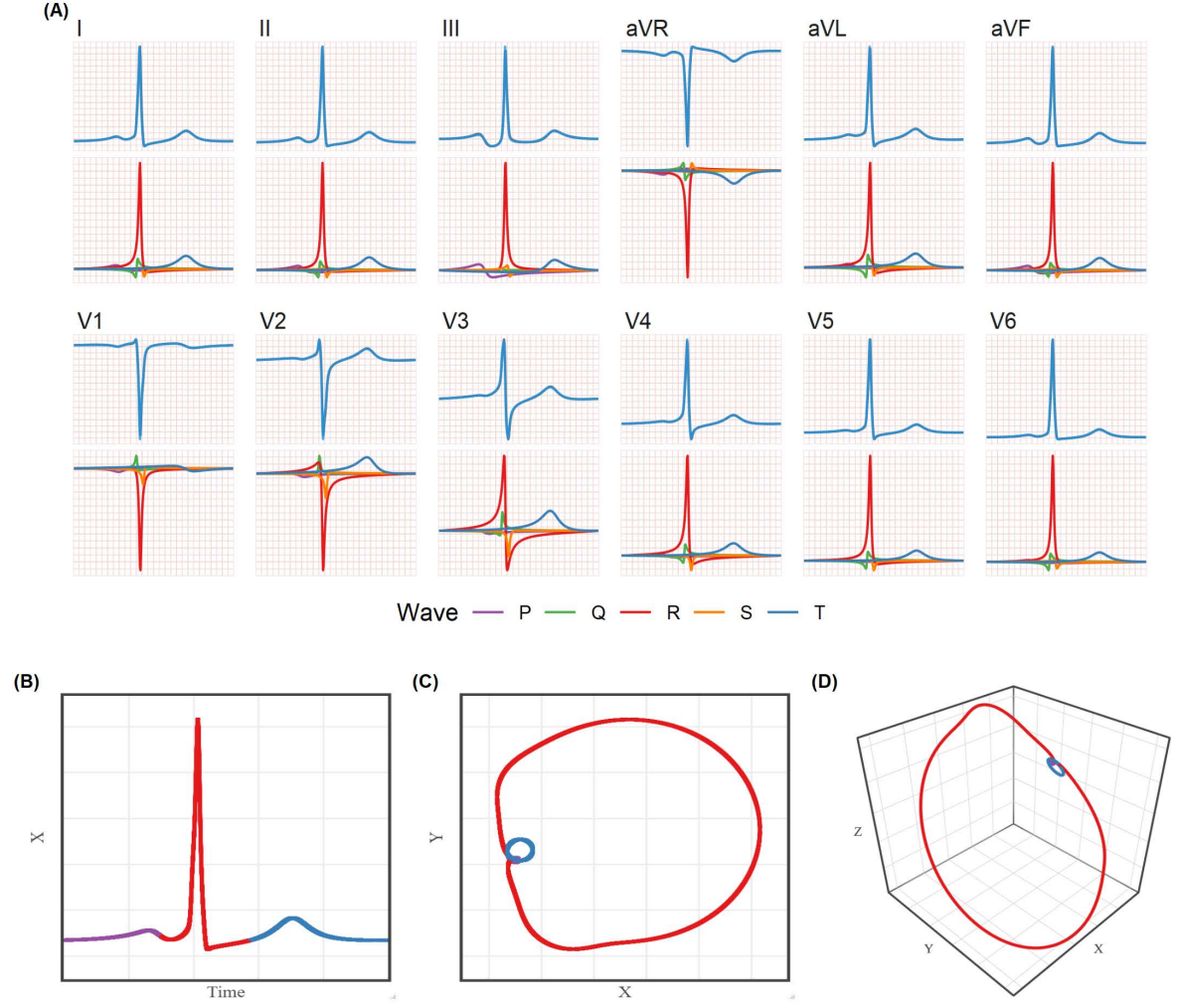
Extended Data Fig. 1: ECG signal from a NORM heartbeat generated by the $3DFMM_{ecg}$ model. (A) 12-lead signals. (B), (C), (D): 1D, 2D and 3D representation of the predicted signal, respectively.



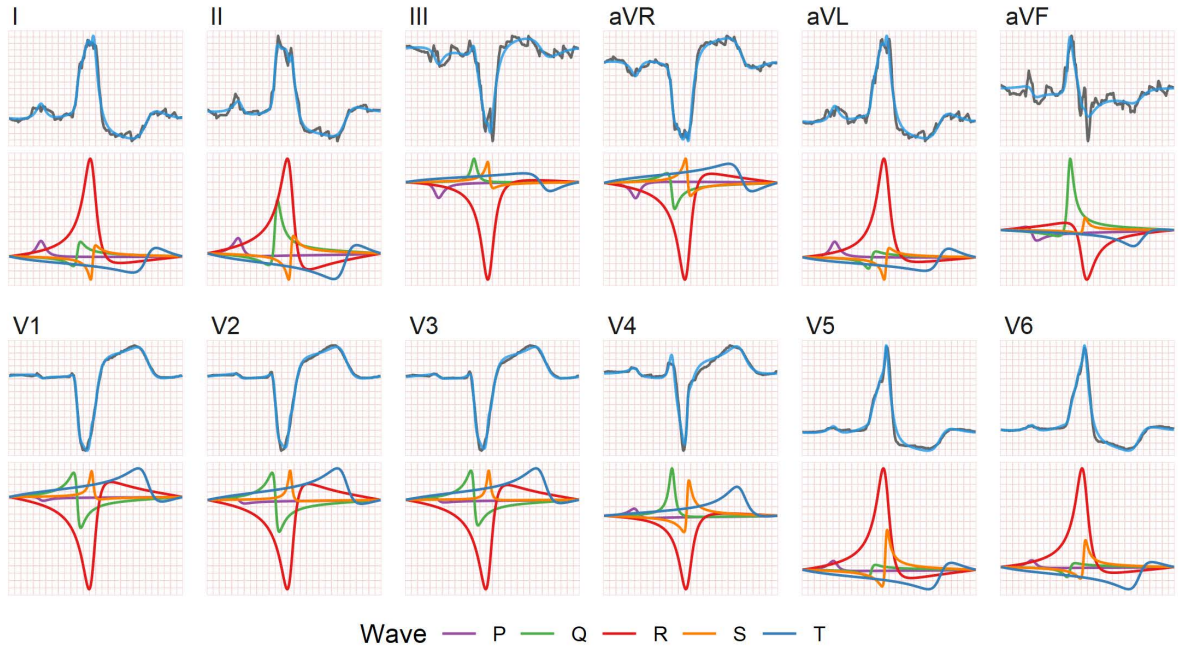
Extended Data Fig. 2: ECG signal from a CLBBB heartbeat generated by the $3DFMM_{ecg}$ model. (A) 12-lead signals. (B), (C), (D): 1D, 2D and 3D representation of the predicted signal, respectively.



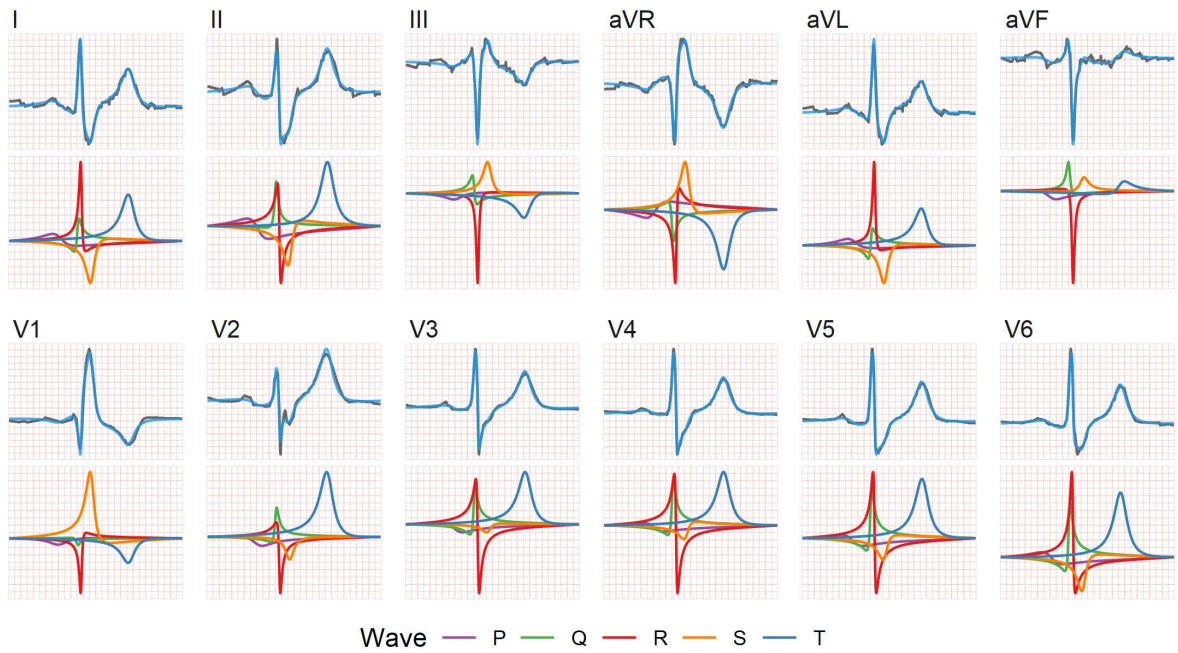
Extended Data Fig. 3: ECG signal from a CRBBB heartbeat generated by the $3DFMM_{ecg}$ model. (A) 12-lead signals. (B), (C), (D): 1D, 2D and 3D representation of the predicted signal, respectively.



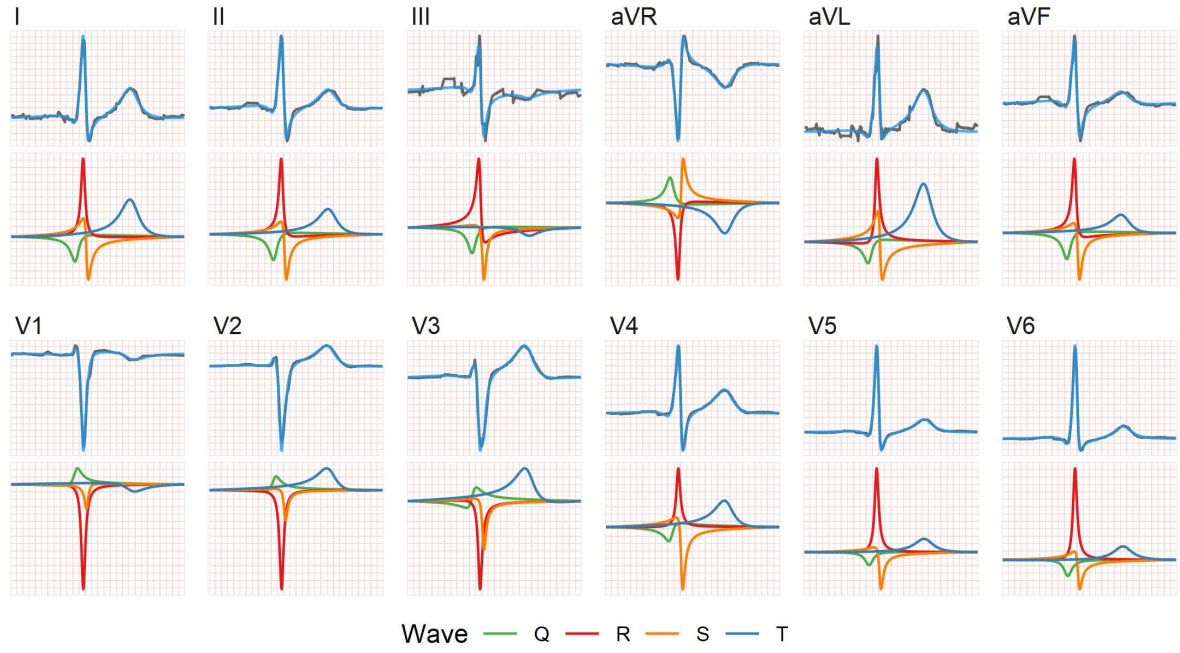
Extended Data Fig. 4: ECG signal from a HYP heartbeat generated by the $3DFMM_{ecg}$ model. (A) 12-lead signals. (B), (C), (D): 1D, 2D and 3D representation of the predicted signal, respectively.



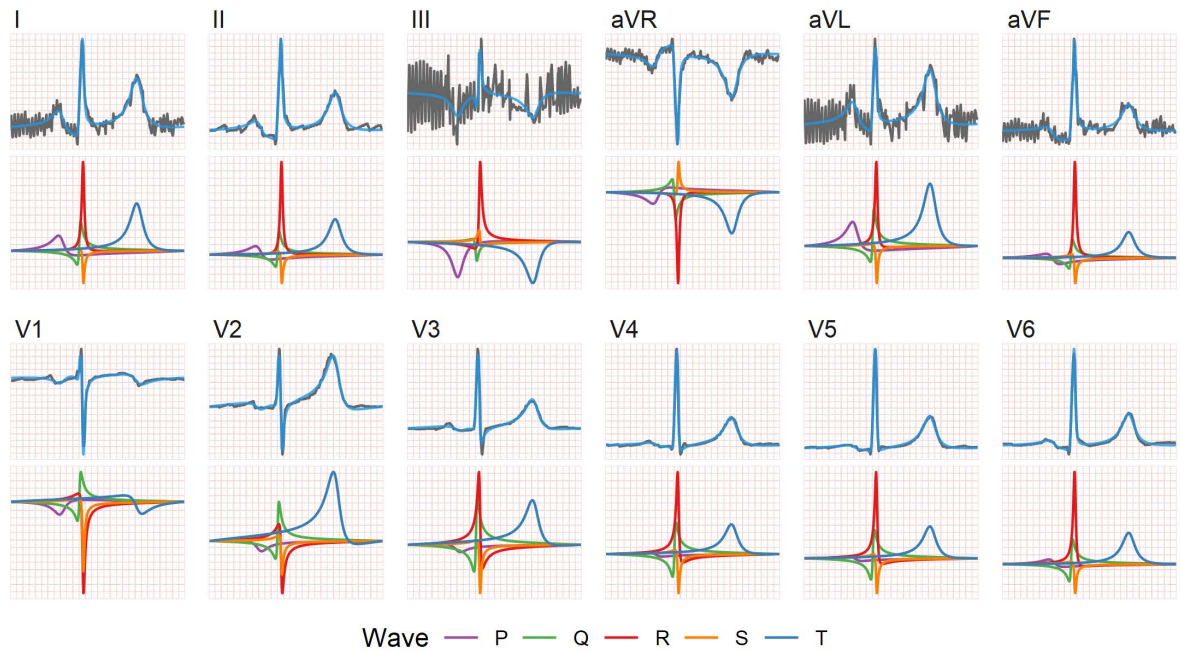
Extended Data Fig. 5: 12-lead ECG signal from patient id 1710 in PTB-XL database, beat n°3. Cardiological diagnostic: CLBBB.



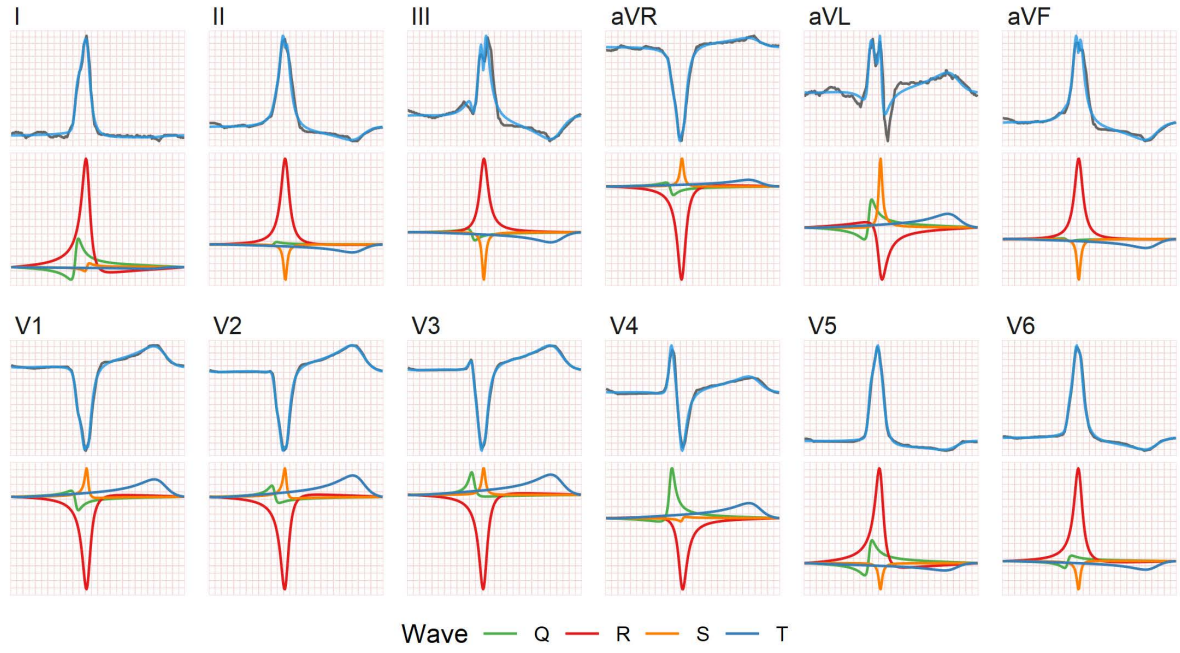
Extended Data Fig. 6: 12-lead ECG signal from patient id 195 in PTB-XL database, beat n° 1. Cardiological diagnostic: CRBBB.



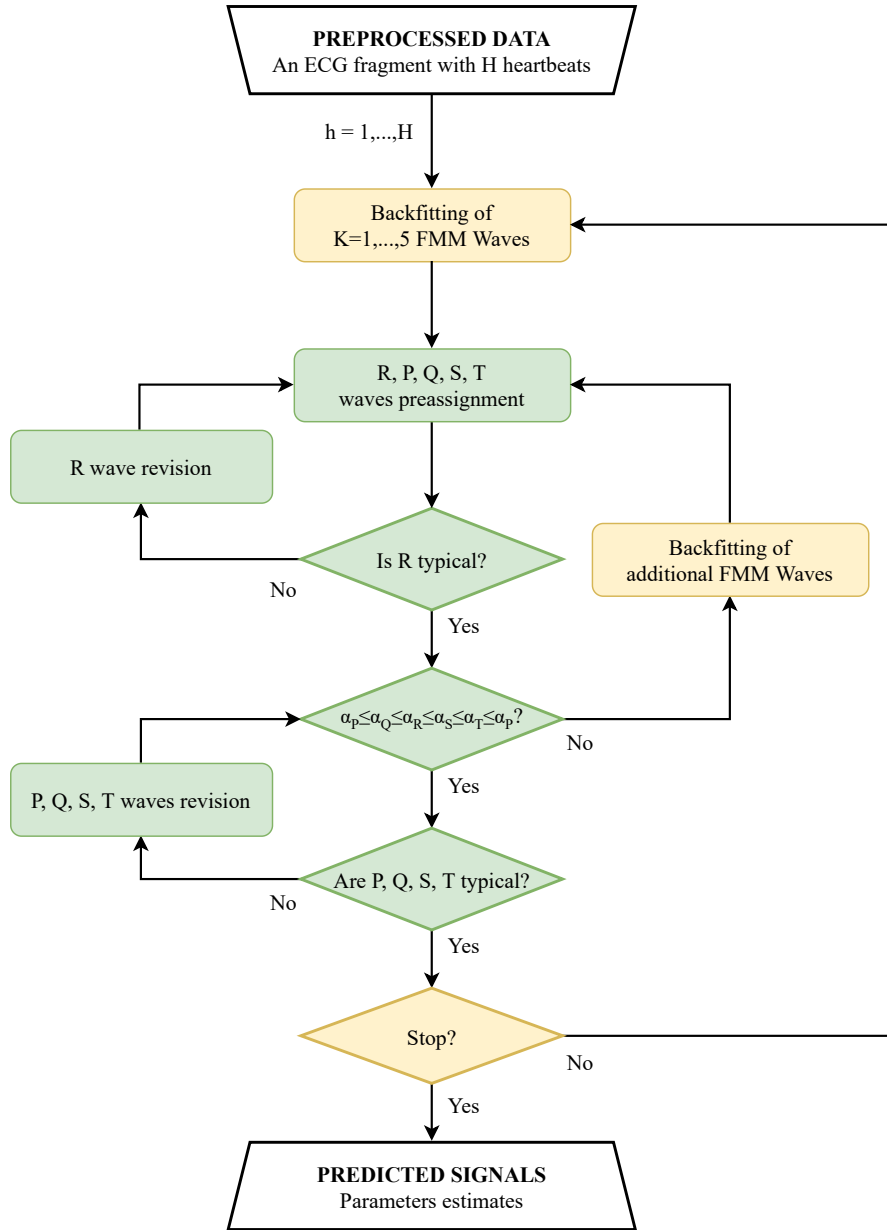
Extended Data Fig. 7: 12-lead ECG signal from patient id 30 in PTB-XL database, beat n°6. Cardiological diagnostic: HYP.



Extended Data Fig. 8: 12-lead ECG signal from patient id 2838 in PTB-XL database, beat n°7. Noisy ECG signal for a NORM subject.



Extended Data Fig. 9: 12-lead ECG signal from patient id 12507 in PTB-XL database, beat n°11. Cardiological diagnostic: Incomplete LBBB. Absence of *P* wave.



Extended Data Fig. 10: Flow chart of the Identification Algorithm. The yellow and green blocks correspond to the M-step and the I-step, respectively. White blocks refer to the inputs and outputs.